A Navier-Stokes Solution for a Bulbous Payload Shroud

Sharad C. Purohit*
Vikram Sarabhai Space Centre, ISRO, Trivandrum, India

The unsteady, compressible Navier-Stokes equations in mass averaged variables are solved for flow past a bulbous shroud. For the freestream Mach number 0.8 and Reynolds number 3.37×10^7/m, a time-dependent computation is performed, using MacCormack's explicit finite-difference scheme with 64×30 grid points. The entire flowfield along the shroud is analyzed to capture a terminal shock and the separation zones. A comparison with available experimental results is reported and evaluation of the unsteady data for surface pressure fluctuations is presented.

Nomenclature

C_p = pressure coefficient
D = forebody diameter
D_1 = Van Driest's damping factor
e = specific energy, $C_vT+0.5\,(u^2+v^2)$
E,F,H = flux vectors, Eq. (2)
J = Jacobian of transformation, $\partial(x,\xi)/\partial(\xi,\eta)$
P = static pressure
$\dot{q}$ = heat flux
SPL = sound pressure level, dB, Re 20 $\mu N/m^2$
t = time
T = temperature
TCH = characteristic time
u,v = velocity components
U = mass averaged dependent variable
ω = vorticity
μ = molecular viscosity
ϵ = eddy viscosity
ρ = density
x,r = polar coordinates
ξ,η = transformed coordinates
δ_{mn} = Kronecker delta
τ_{mn} = stress tensor

Subscripts

∞ = freestream conditions
w = surface conditions
m,n = indicial notations, Eq. (1)

Introduction

IN recent years, the prediction of flow-induced unsteady oscillations around an aerospace vehicle has gained prominence. While the strategic demands of the vehicle require a critical analysis of the associated mission parameters, the fundamental knowledge of the fluid physics is of major concern to the designers. The bulbous shaped shroud falls in one such category, where an increase in payload volume for a satellite launch vehicle offers numerous attractive dividends. The estimation of flowfield characteristics around such configurations is of considerable practical, as well as research, interest. For the ascent flight, during the transonic speed range, the study is particularly important because of the inherent phenomenon such as shock movements frequently coupled with a substantial dynamic pressure. These parameters implicitly depend on the intensity of the vorticity components of the turbulence, the strength of the shock, and the mechanism of their interaction, all of which are linked to specific body shapes. For a geometry such as blunt nose cone-cylinder-flare-cylinder (the bulbous payload shroud shown in Fig. 1), the probable regions of flow separation impose an additional complexity due to aerodynamic and structural design aspects.[1-4] Furthermore, as the boundary layer in the boattail region is comparatively thicker, the evaluation of viscous-inviscid interaction becomes necessary.

The flow oscillations and the possible separation zones along the shroud introduce yet another serious concern in the form of aeroacoustic noise.[5,6] The maximum acoustic field strength for such a shroud is observed during the transonic phase of the flight with the high dynamic pressure conditions on the vehicle. This is primarily reflected as surface pressure fluctuations causing undesirable loads and buffet forces. As pointed out by Karamcheti,[7] to quantify the behavior of such acoustic source, the basic fluid mechanics of real, unsteady flow should be utilized to gain physical insight into what the flow characteristics and the nature of fluctuations are like. In this context, the objective of the present preliminary investigation is to analyze the time-dependent pressure fluctuations due to the fluid-surface interaction and to determine the critical "noise" parameter, the sound pressure levels (SPL).

Even though the task is of prime importance, the complete analysis of the flowfield around the bulbous shroud is a real challenge. The computational and experimental studies are the two common approaches to solve such problems. Complementing the experimental efforts,[8] this paper describes a computational approach. The prime objectives are to establish the credibility of the numerical procedure and to compare the results with the available experimental data.[8]

A survey of the literature reveals substantial efforts in this area.[9-14] However, for the various body geometries, the available data are so sparse that a definite conclusion regarding the flow aspects of a bulbous shroud can not be reached easily. Thus, in order to obtain a fruitful result, the separated

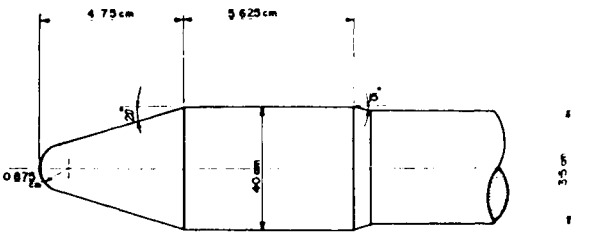

Fig. 1 The bulbous payload shroud.

Received May 13, 1985; revision received Jan. 11, 1986.

*Scientist, Applied Mathematics Division. Member AIAA.

flow, the shock location, and their domain of influence demand a systematic and step-by-step in depth study. We have considered as a typical case a freestream Mach number 0.80, a Reynolds number 3.37×10^7/m, and a zero angle of incidence. For this set of data, a shock-induced separation is located just downstream of the cone-cylinder junction.[8] The aim is to compute the mean and the fluctuating flow along the shroud, the zones of separation, a Gaussian distribution for the unsteady pressure data, and the range of sound pressure levels, dB and the corresponding frequencies.

Analysis

Based on the experimental data from the wind tunnel test facility at zero angle of incidence, the mean flow along the bulbous shroud appears to be, in general, axisymmetric. Therefore, to understand the basic fluid physics, a numerical solution of the unsteady, compressible Navier-Stokes equations is attempted along a shroud generator. These equations contain all the terms required to solve viscous-inviscid interaction and the separation region at high Reynolds number. Neglecting body forces, the governing equations, in mass averaged variables are written in the following form:

$$(\rho)_{,t}+(\rho u_n)_{,n}=0$$

$$(\rho u_m)_{,t}+[(\rho u_m)u_n+P\delta_{mn}-\tau_{mn}]_{,n}=0$$

$$(\rho e)_{,t}+[(\rho e)u_n+\dot{q}_n-u_m\tau_{mn}]_{,n}=0 \qquad (1)$$

where the values of the stress tensor and heat fluxes are the total values. With the help of the perfect gas law, Sutherland's formula, and a suitable turbulence model, the system of equations is closed.

The fluid motion described by the aforementioned equations is to be solved along a bulbous payload shroud, Fig. 1. The forebody diameter of the model is 0.04 m, whereas the afterbody diameter is 0.035 m. The boattail angle is 15 deg measured clockwise from the axis with reference to the oncoming flow direction. For the blunt nosed cone, the inclination at the forebody junction is $(\pi-20$ deg) and the total length of the shroud from the stagnation point to the boattail is 0.083 m. These subscale dimensions were chosen after considering the blockage and compatibility conditions with the model system support of the wind tunnel.[8]

One of the controlling factors for the numerical simulation is the proper selection of the coordinate system and grid arrangement. In order to avoid any interpolation during computation, the effective way is to opt for body-oriented grids.

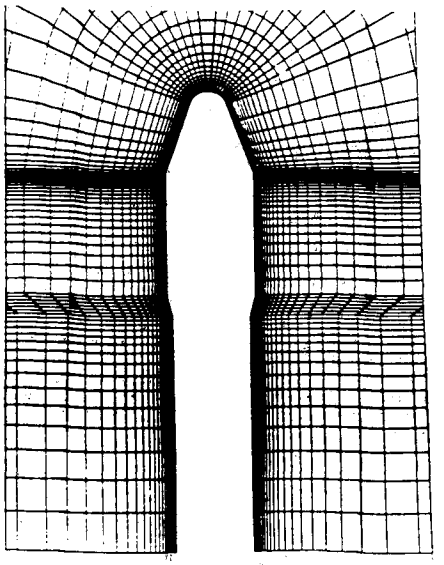

Fig. 2 Mesh system of the shroud.

We discretize the shroud by 64 points for the cylindrical polar coordinate system. The origin of the x-r plane is at the stagnation point with the positive x-direction along the shroud. In anticipation of the close presence of the shock to cone-cylinder junction, 20 grid points defining the forebody were exponentially stretched for adequate resolution (see Fig. 2). Similarly, 15 grid points defining the afterbody also were stretched up to four times the diameter. For the blunt nose, 11 grid points were uniformly placed at an angular interval of 6.1 deg and the first point was placed at the mirror image location of the second grid point to accommodate the symmetric boundary conditions. Using these surface nodes as reference points, the normal coordinates are then described by 30 field points (x,r) extending outwards to six times the forebody diameter. The finer mesh near the surface helps resolve the viscous effects; the courser mesh helps in reducing the computer time. The minimum mesh sizes in the normal, and along the solid surface, were 8.138×10^{-5} m and 6.047×10^{-4} m, respectively. Using the non-singular Jacobian, J, the Navier-Stokes equations in the transformed computational plan (ξ,η) were rewritten as

$$\frac{\partial U}{\partial t}+\left[\xi_x\frac{\partial E}{\partial\xi}+\frac{1}{\xi}\xi_\gamma\frac{\partial}{\partial\xi}(\xi F)\right]+\left[\eta_x\frac{\partial E}{\partial\eta}+\frac{1}{\xi}\eta_\xi\frac{\partial}{\partial\eta}(\xi F)\right]=\frac{H}{\xi} \qquad (2)$$

where $U=[\rho,\rho u,\rho v,\rho e]^T$ and E, F, H are the vector fluxes. While the governing equations are solved in the computational space, the knowledge of inverse Jacobian helps interpret the results in the physical space.

For the present preliminary investigation, a two-layer algebraic model[15] has been used as a turbulence closure. This model, which utilizes vorticity distribution to determine the scale lengths, has been used previously and is reputed to offer acceptable engineering solutions.[16,17]

In the inner region, the eddy viscosity is given by

$$\epsilon_i=(0.4\,D_1L)\rho\,|\omega| \qquad (3)$$

where ω is the vorticity function, L is the distance normal to the bulbous shroud, and D_1 is the Van Driest's damping factor

$$D_1=1-\exp\left(-\sqrt{\frac{\rho_w|\omega_w|}{\mu_w}}\,\frac{L}{26}\right)$$

In the outer region,

$$\epsilon_0=0.0168(1.6)F_wF_{KEF} \qquad (4)$$

The coefficient F_w is calculated as the minimum of the following two values

$$(i)L_{\max}F_{\max}, \qquad (ii)0.25L_{\max}\max(\sqrt{u^2+v^2})/F_{\max}$$

The scale length $L_{\max}$ is the maximum value of L when the function $F(=LD_1|\omega|)$ attains its maximum, $F_{\max}$. The Klebanoff intermittency correction factor is given by

$$F_{KIF}=\left[1.0+5.5\left(0.3\frac{L}{L_{\max}}\right)^6\right]^{-1} \qquad (5)$$

The effective viscosity is then given by

$$\epsilon=\min(\epsilon_i,\epsilon_0) \qquad (6)$$

Numerical Procedure

The schlieren photographs for the experimental results show a significant variation in the flow around the shroud up to one forebody diameter. Beyond this distance, the flowfield

changes are very small. This observation indicates that the primary physical phenomenon consisting of the propagation of pressure waves and vortices limit the flow variables to the asymptotic values in the farfield. Thus, if the boundary conditions are specified at a sufficiently large distance from the shroud, the overspecification is generally acceptable.[18] Initially the shroud is assumed to be immersed completely in the uniform flow. The upstream boundary conditions are merely freestream values whereas at the downstream boundary, the gradient of properties is zero. At the shroud surface, no-slip and adiabatic conditions were imposed; near the axis symmetric conditions were used.

The numerical scheme used for the present study is MacCormack's explicit finite-difference scheme, which involves a combination of alternating forward and backward differences for the predictor and corrector steps.[19] Fourth-order pressure damping terms also were introduced during the computation, which are effective only in the large pressure gradients associated with the shock wave.[20] A conservative choice of the CFL number (0.80) was made to achieve a stable numerical solution. The computer used for the analysis was CDC CYBER 170/730 with 131K memory available to the users. The characteristic time, TCH (=forebody diam/freestream velocity), was 1.53×10^{-4} s. To solve the transformed Navier-Stokes equations at 64×30 grid points, the data processing rate (CPU time per grid point, per time iteration) of 3.488×10^{-3} s was attained with almost all the memory utilized. Once the initial phase of computation was over, and some periodicity in the flow characteristics was observed, the study of flowfield data was attempted, to assess the separation zones and shock locations and to compute the sound pressure levels and the frequencies.

Results and Discussion

The comparison of experimental data and the numerical solution offers validation of the computational procedure as well as guidelines for the subsequent analysis. The experimental results[8] are essentially parametric in nature and provide the pressure measurements at selected stations.

The computed surface pressure data along the shroud was analyzed for the time mean and the root mean square (rms) values using the following relations:

$$\bar{C}_{pk}=\frac{1}{TM}\int_{t}^{t+TM} C_{pk,m}\,dt \tag{7}$$

$$\langle C_{pk}^2\rangle=\left[\frac{1}{TM}\int_{t}^{t+TM} C_{pk,m}^2\,dt-\left\{\frac{1}{TM}\int_{t}^{t+TM} C_{pk,m}\,dt\right\}^2\right]$$

$$k=1,2\ldots64,\qquad m=1,2\ldots3600 \tag{8}$$

where $C_{pk,m}$ corresponds to pressure coefficients at the kth node at time $m\Delta t$ ($\Delta t=2.146\times10^{-6}$ s) and TM is the total time period, equal to 0.0076 s and is considered after the 8000 time step computation is over. Since the time increment for the pressure values is very small, the integral procedures Eqs. (7) and (8) were adopted. The results are shown in Figs. 3 and 4. The experimental values of mean pressure are taken from Ref. 8. The computed results compare quite well with the experiment along the entire length of the shroud except at the cone-cylinder junction where the maximum expansion occurs. Near the stagnation point and on the spherical region, a steep fall in pressure coefficients was registered, which is partially recovered along the cone. The experimental values also agree to this trend from the station $x/D=0.22$ onwards where the first pressure measurement was made. On the forebody cylinder, just after the cone-cylinder junction, the flow characteristics exhibit a pressure plateau indicating separation. In the boattail region, the expansions and compressions are comparatively mild, and the computed results show a remarkable agreement with the experimental data. Along the afterbody, the pressure

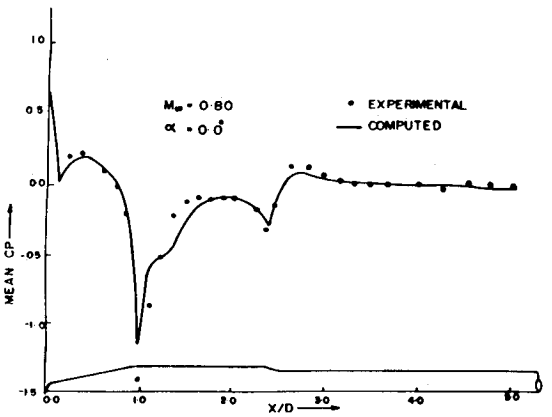

Fig. 3 Comparison of CP distribution.

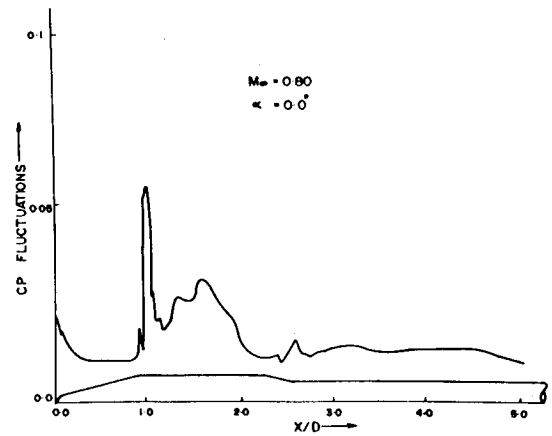

Fig. 4 RMS pressure fluctuations along the shroud.

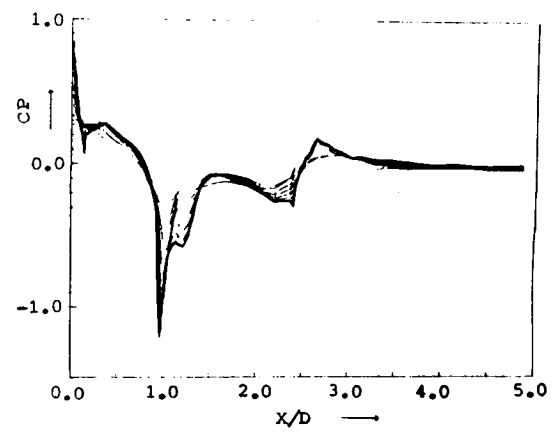

Fig. 5 Terminal shock wave location.

coefficients recover, as expected, to their freestream values within one forebody diam distance. The RMS pressure coefficient fluctuations, however, show a high peak and sharp variation near the cone-cylinder junction where a shock wave might be located.

Significant insight into this phenomenon is demonstrated in Fig. 5. The pressure jumps across the shock near the cone-cylinder junction are self evident in the graph. The result tallies qualitatively with the flow patttern indicated by the schlieren pictures.[8] A closer look into these pressure jumps shows that the shock formation is due to the merger of many compression waves ahead of the separation bubble. The shock wave was resolved within four mesh points. However, this resolution can be refined further by introducing more grid

points, which strongly affects the available computational resources.

In Fig. 6 we present a skin-friction coefficient distribution along the shroud. It can be observed that strongly attached flow near the cone-cylinder junction and an expansion due to the typical shroud geometry gives way to a separation following a terminal shock wave of the supersonic pocket. This separation is confined to a short distance and the flow reattaches at $x/D=1.572$. For a freestream Mach number of 0.80, the present case, a similar interesting flow pattern is reported by Ramaswamy.[21] Along the boattail region, yet another local separation results, due to a sharp discontinuity in the longitudinal curvature. The flow separates at $x/D=2.41$ and the separation point is confined to a very small interval during the time-dependent computation. A glimpse of the flowfield structure is given in Figs. 7 and 8 through instantaneous velocity field along the shroud and in the boattail region. A thickening boundary layer and a strong recirculating flow at the boattail afterbody junction can be noticed distinctly. Computing the local Mach numbers we note that a supersonic zone, in an otherwise high subsonic flow, is formed near the cone-cylinder junction of the shroud. This zone extends from $x/D=0.95$ to $x/D=1.22$ (and up to maximum height of $r/D=0.716$ at $x/D=1.0265$) compared to the experimental values of $x/D=0.93$ to $x/D=1.28$. The computed critical pressure coefficient $c_p^*=-0.462$ compared with the value -0.425 deduced from the experimental data. The pressure values in the boattail region lie much below the critical level, and thus flow never crosses the sonic limit.

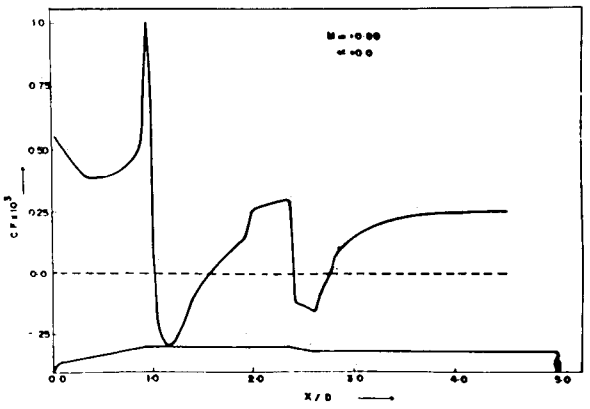

Fig. 6 Skin friction distribution.

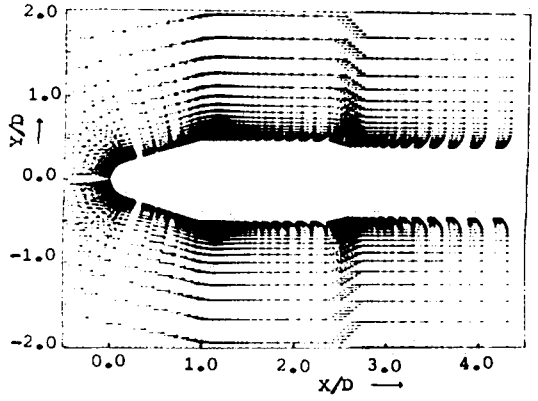

Fig. 7 Instantaneous velocity field along the shroud.

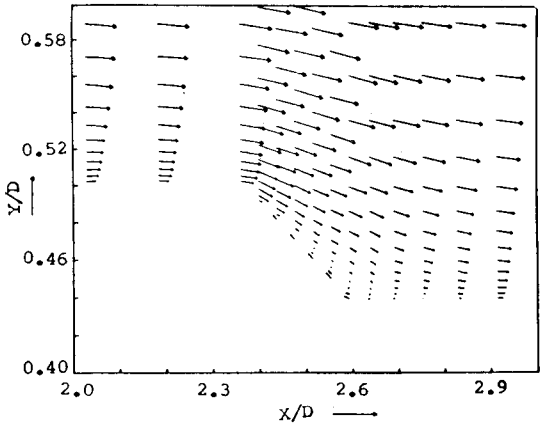

Fig. 8 Instantaneous velocity field for the boattail region.

The prime objective of solving the Navier-Stokes equations was to study the unsteady flowfield behavior, particularly that of the surface pressure along the shroud. As mentioned earlier, the shroud surface was discretized by 64 nonuniformly spaced grid points. At each grid point during computation a sufficient amount of time-dependent data was stored for frequency analysis. In order to explore the sensitivity of unsteadiness, four sample stations along the shroud are used, viz.,

1) $x/D=0.968$ (near cone-cylinder, shock)
2) $x/D=1.146$ (forebody cylinder, separation)
3) $x/D=2.467$ (boattail, separation)
4) $x/D=2.593$ (boattail-cylinder, separation).

A set of histograms for the surface pressure distribution at the stations is shown in Fig. 9 as a function of computed nondimensional time, t/TCH. The axes are not equally scaled and are enlarged considerably to emphasize the variation. Because of our choice for the algebraic turbulence model, the oscillations in the pressure signature might be affected.[22] The assessment of such contributions was not attempted in the present investigation.

Before the analysis of the amplification factor and sound pressure levels was initiated we wanted to ensure that the data are free from transitional phase, i.e., the pressure values are representative of the data, if the computation had been continued for a very long time. To achieve this objective, a statistical approach was attempted from the large data sets with the last 3600 sets of values considered. Out of these data sets, different subsets were tested and the normalized Gaussian distributions were plotted. It was concluded that if the last 2000 points were taken, the distribution was normal at most of the locations (Fig. 10). While the data in the boattail separation region and everywhere in the attached flow regions follow a Gaussian distribution,[23] a striking contrast is observd for the forebody cylinder pressure data. Instead of characterizing 68% data dispersion within the first unit of standard deviation, 99%, at $x/D=0.968$ and 90%, at $x/D=1.146$, data dispersions were exhibited. This suggests that irrespective of the large computations, the data variations at the shock location is restricted to a smaller domain of variation. This, in turn, may trigger an increase in the "noise" levels and might affect the structural and aerodynamic design criteria.

A spectral analysis for all possible modes of oscillations was carried out using a two-hundred-term Fourier series. The frequencies for which the assessment was done are multiples of the fundamental frequency, 130 Hz. For pressure fluctuations, the sound pressure levels were computed in terms of the RMS pressure of 20 $\mu N/m^2$ (Fig. 11). The functional values of SPL reveal that, in the boattail region, the significant peaks appear at approximately 8.2 KHz frequency. However, at station $x/D=0.968$, the SPL peak is observed at 1 KHz frequency, and at the rest of the points in the first local separation bubble the highest SPL never seemed to cross 0.3 KHz. To substantiate our earlier results we plot the SPL for all the grid point locations near the shock in Fig. 12. The SPL value increases gradually in the local supersonic pocket and attains its maximum value of 150.06 dB at $x/D=1.02$ which is probably the closest ordinate to the exact terminal shock location.

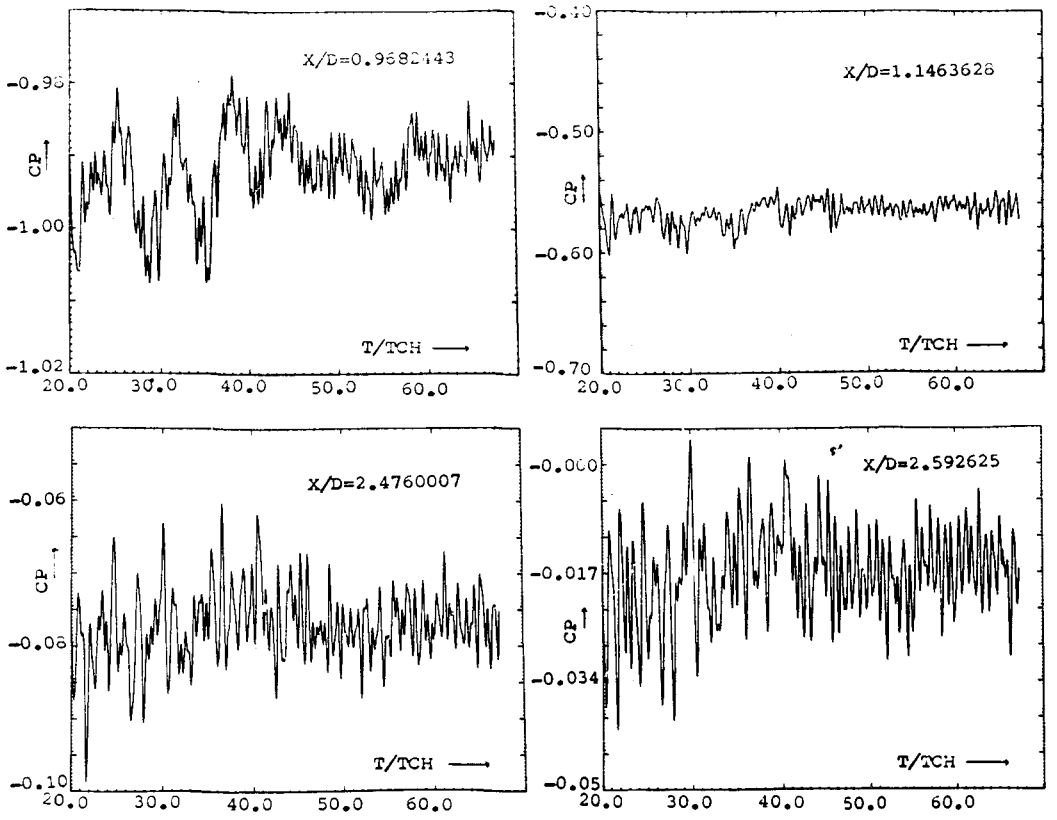

Fig. 9 Typical histogram of pressure oscillations.

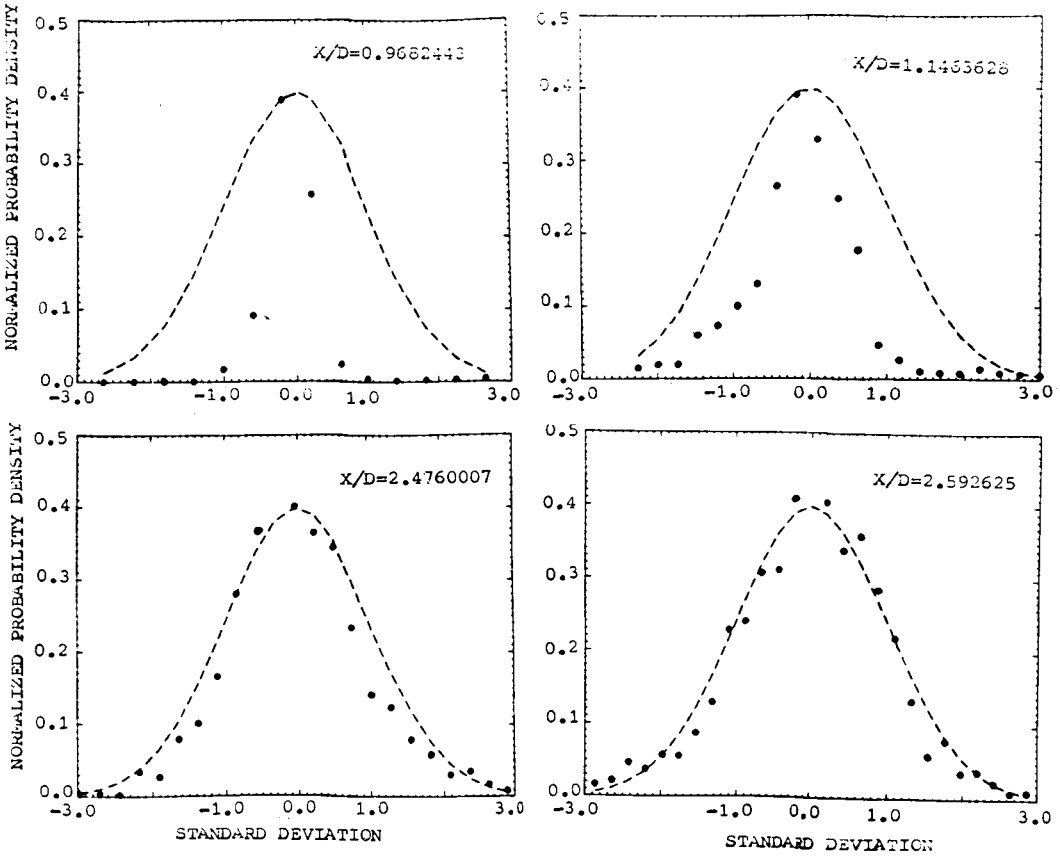

Fig. 10 Probability density distribution at selected stations.

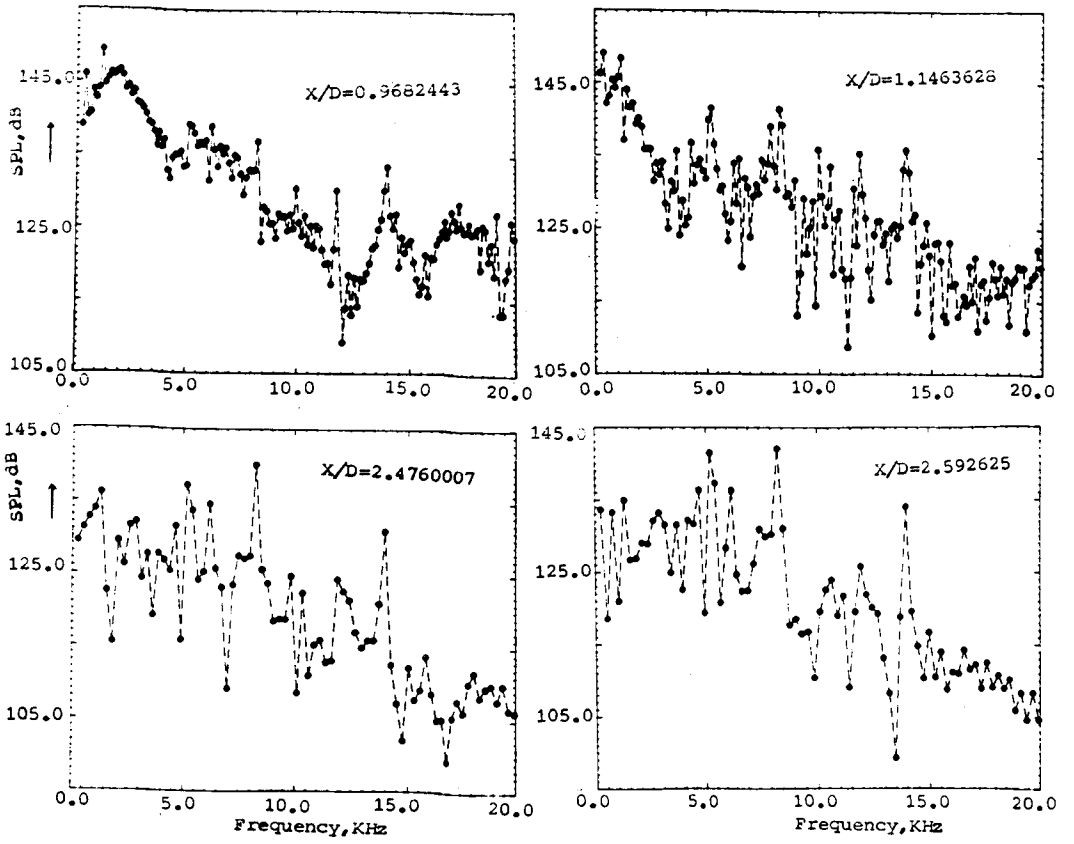

Fig. 11 Spectral analysis.

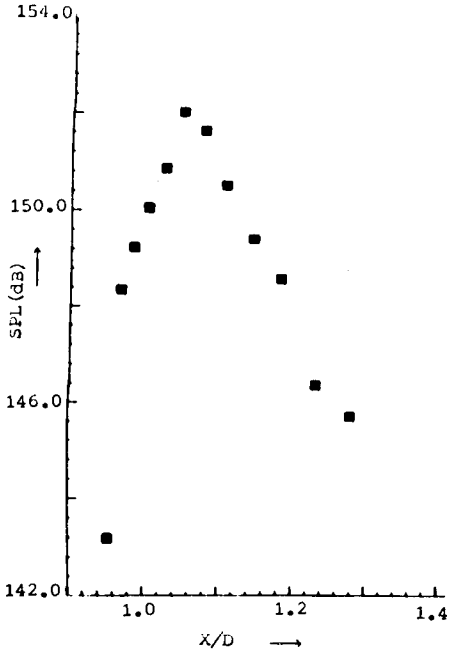

Fig. 12 Sound pressure levels near shock location.

The SPL numbers provided in the graph are at the discrete mesh points and a continuous function can be predicted easily. By considering more grid points, the nature of the terminal shock wave and its interaction with the turbulent boundary layer can be recalculated, and it is anticipated that the form of the critical noise parameter will not be significantly different.

Conclusions

For a freestream Mach number of 0.80 and a Reynolds number of 3.37×10^7/m, the computation of unsteady, compressible Navier-Stokes equations is carried out and a good comparison with experimental results is established. Qualitative agreement is obtained for the general flowfield, including the locations of terminal shock and separation zones. Using a Gaussian distribution, the appropriate unsteady pressure data are utilized to calculate the SPL and the corresponding frequencies. The time-dependent calculation reveals that around the cone-cylinder junction near the shock the SPL values are high and coupled with the low frequency.

Acknowledgment

The author wishes to thank Dr. T.S. Prahlad for several helpful discussions throughout the course of this work.

References

[1]NASA Special Project Report, "Buffeting During Atmospheric Ascent," *NASA Special Vehicle Design Criteria*, NASA SP 8001, Nov. 1970.

[2]Rainey, A. G., "Progress on the Launch Vehicle Buffeting Problem, *Journal of Spacecraft and Rockets*, Vol. 2, March 1965, pp. 289-299.

[3]Pearcey, H., Osborn, J., and Haines, A. B., "The Interaction Between Local Effects at the Shock and Rear Separation," AGARD-CP-35, 1968.

[4]Hankey, W. L. and Shang, J. S., "Analysis of Self-Exited Oscillations in Fluid Flow," AIAA Paper 80-1346, July 1980.

[5]Lighthill, M. J., "On Sound Generated Aerodynamically," Proceedings of the Royal Society of London, Series A, Vol. 211, 1952, pp. 564-587.

[6]Hayden, R. E., Kadman, Y., Bliss, D. B., and Afrik, S. A., "Diagnostic Calculations of Airframe-Radiated Noise," *Progress in Astronautics and Aeronautics*, Vol. 45, 1976, pp. 179-201.

[7]Karamcheti, K., "Airframe and Aerofoil Noise-Panel Discussion," *Progress in Astronautics and Aeronautics*, Vol. 45, 1976, pp. 441-443.

[8]Ahmed, S., "Flow Visualization Studies at Transonic Speeds on Heat Shield Configurations," NAL-TWT-1-36, 1984.

[9]Diewart, G. S., "Numerical Simulation of Three-Dimensional Boattail Afterbody Flow Field," *AIAA Journal*, Vol. 19, May 1981, pp. 582–588.

[10]Wington, L. and Holt, M., "Viscous-Inviscid Interaction in Transonic Flow," AIAA Paper 81-1003 CP, June 1981.

[11]Horstman, C. C., "Prediction of Separated Axisymmetric Trailing Edge Flows at Transonic Mach Number," *AIAA Journal*, Vol. 21, Sept. 1983, pp. 1255–1261.

[12]Shrewsbary, G. D. and Tassa, Y., "Numerical Simulation of Transonic Flow about Isolated Afterbody," AIAA Paper 83-0498, Jan. 1983.

[13]Nietubicz, C. J., Inger, G. R., and Danberg, J. E., "A Theoretical and Experimental Investigation of a Transonic Projectile Flow Field," *AIAA Journal*, Vol. 22, Jan. 1984, pp. 35–41.

[14]Khosla, P. K., and Lai, H. T., "Global PNS solution for Subsonic Strong Interaction Flow over a Cone-Cylinder-Boattail Configuration," *Computers and Fluids*, Vol. 11, No. 4, 1983, pp. 325–339.

[15]Baldwin, B. S. and Lomax, H., "Thin Layer Approximation and Algebraic Model for Separated Turbulent Flows," AIAA Paper 78-257, Jan. 1978.

[16]Purohit, S. C., Shang, J. S., and Hankey, W. L., "Effect of Suction on the Wake Structure of a Three-Dimensional Turret," AIAA Paper 83-1738, July 1983.

[17]Shang, J. S., "Numerical Simulation of Wing-Fuselage Aerodynamic Interaction," *AIAA Journal*, Vol. 22, Oct. 1984, pp. 1345–1353.

[18]Purohit, S. C., Shang, J. S., and Hankey, W. L., "Numerical Simulation of Flow around a Three-Dimensional Turret," *AIAA Journal*, Vol. 21, Nov. 1983, pp. 1533–1540.

[19]MacCormack, R. W., "The Effects of Viscosity in Hypervelocity Impact Cratering," AIAA Paper 69-354, May 1969.

[20]MacCormack, R. W. and Lomax, H., "Numerical Solution of Compressible Viscous Flows," *Annual Review of Fluid Mechanics*, Vol. 11, 1979, pp. 289–316.

[21]Ramaswamy, M. A. and Rajendra, G., "Experimental Investigation of Transonic Flow Past a Blunt Cone-Cylinder," *Journal of Spacecraft and Rockets*, Vol. 15, Feb. 1978, pp. 120–123.

[22]Shang, J. S., "An Assessment of Numerical Solutions of the Compressible Navier-Stokes Equations," *Journal of Aircraft*, Vol. 22, May 1985, pp. 353–370.

[23]Purohit, S. C., "Analysis of Unsteady Pressure Data for PSLV Heat Shield," VSSC:ADDG:APMD:PSLV:26: 85, July 1985.